Nanoscale

Accepted Manuscript

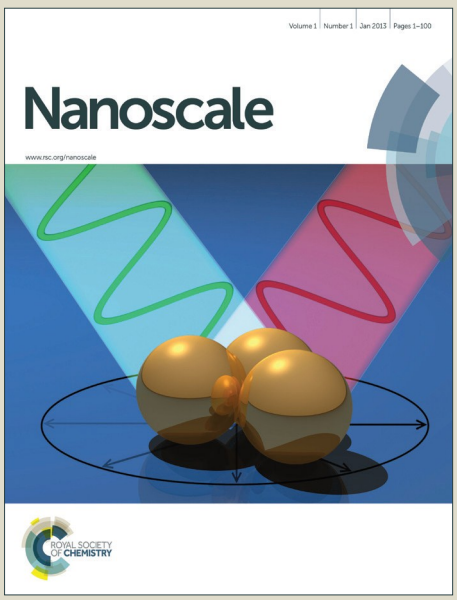

ROYAL SOCIETY OF CHEMISTRY

www.rsc.org/nanoscale

Journal Name

RSCPublishing

ARTICLE

In situ Synthesis of Large Area Boron Nitride/Graphene Monolayer/Boron Nitride Film by Chemical Vapor Deposition

Cite this: DOI: 10.1039/x0xx00000x

Received 00th January 2012,
Accepted 00th January 2012

DOI: 10.1039/x0xx00000x

www.rsc.org/

Qinke Wu[1], Sungkyu Jang[1], Sangwoo Park[1], Seong Jun Jung[1], Hwansoo Suh[2], Young Hee Lee[4*], Sungjoo Lee[1,5,6*] and Young Jae Song[1,4,7*]

We describe the successful in situ chemical vapor deposition synthesis of a graphene-based heterostructure in which a graphene monolayer is protected by top and bottom boron nitride films. The boron nitride film/graphene monolayer/boron nitride film (BGB) was found to be a mechanically robust and chemically inert heterostructure, from which the deleterious effects of mechanical transfer processes and unwanted chemical doping under air exposure were eliminated. The chemical compositions of each film layer were monitored ex situ using UV-visible absorption spectroscopy and X-ray photoelectron spectroscopy, and the crystalline structures were confirmed using transmission electron microscopy and selected-area electron diffraction measurements. The performance of the devices fabricated using the BGB film were monitored over six months and did not display large changes in the mobility or Dirac point, unlike the conventional graphene devices prepared on a SiO_2 substrate. The in situ-grown BGB film properties suggest a novel approach to the fabrication of commercial-grade graphene-based electronic devices.

Introduction

As research into the properties of pristine graphene has advanced, the focus has shifted to two-dimensional heterostructures in which graphene is stacked with various two-dimensional transition metal dichalcogenide layers, such as MoS_2, WS_2, $MoSe_2$, or WSe_2, or with hexagonal boron nitride (h-BN) in a precisely selected sequence. These heterostructures display unusual properties and have enabled the exploration of new phenomena.[1–6] h-BN, in particular, provides an ideal insulating material for fabricating heterostructures with graphene because its surface is atomically smooth, it is chemically inert without dangling bonds, and its lattice constant is similar to the lattice constant of graphene.[5,7] To protect the intrinsic properties of graphene and improve its device carrier mobility, layer-by-layer stacking methods are used to prepare graphene-based vertical heterostructure devices with h-BN. Recently, Dean *et al.* transferred graphene onto the surfaces of h-BN/SiO_2/Si substrates and measured a very large room-temperature mobility (~60,000 $cm^2 V^{-1}s^{-1}$) compared to the mobility measured in a graphene layer without h-BN.[5] Wang *et al*. deposited one additional h-BN film onto the surface of a graphene/h-BN/SiO_2 heterostructure sample to fabricate a 1-D contact device.[7] This device showed a high mobility (~140,000 $cm^2 V^{-1}s^{-1}$) at room temperature that approached the intrinsic mobility while yielding chemical robustness in air. Although this transfer method can preserve the intrinsic properties of exfoliated graphene, several technical hurdles have yet to be overcome: (1) the structure size is limited to the micrometer scale, precluding many commercial applications; (2) residues may be captured at the interface between the graphene and h-BN layers, which can degrade the graphene device properties; and (3) it is almost impossible to control the exact stacking orientations. Luckily, chemical vapor deposition (CVD) methods may potentially address all of these problems.

The sequential synthesis of large-area h-BN/graphene or graphene/h-BN structures has been reported previously. Zheng *et al.* reported that the h-BN can be directly grown on a graphene/Cu structure for a PMMA residue to avoid touching on the graphene surface with the top h-BN surface.[8] Graphene is a unique carbon honeycomb monoatomic layer with sp^2 hybridization, so it has no permanent polarity or surface dangling bonds (unpaired electrons). Graphene, therefore, offers an ideal surface at which to study van der Waals attraction. Recently, Wang *et al.* reported that graphene can be grown directly onto CVD-grown h-BN/Cu substrates.[9] Transfer of a sample onto a SiO_2/Si substrate for device fabrication can avoid the preparation of dangling bonds or charged impurities on the SiO_2/Si substrate. Water, which can alter the graphene electronic properties, is not captured between the graphene and SiO_2/Si surfaces using this method.[10] Here, we offer an advanced method for protecting a large-area graphene monolayer by sequentially growing BN/graphene monolayer/BN (BGB) films on copper substrates using low-pressure chemical vapor deposition (LP-CVD) methods. The BGB films were guaranteed to be high-quality during transfer

processes conducted in air or during device fabrication steps. During the synthesis process, the chemical composition and bonding properties of the structure were investigated using UV-visible spectroscopy, scanning electron microscopy (SEM), and X-ray photoelectron spectroscopy (XPS) methods. High-resolution transmission electron microscopy (HR-TEM) studies and selected-area electron diffraction (SAED) methods were used to check the structure crystallinity. Finally, we fabricated a BGB sample to form a device and traced its carrier mobility and Dirac point over six months under exposure to air. The results of these studies revealed that both the carrier mobility and the Dirac point did not vary significantly, indicating that the BGB sample was chemically inert, stable, and suitable for use in commercial applications.

Experimental

Electrochemical polishing of the Cu foil

Pristine copper foil surfaces are not flat and feature many wavy structures and particles that are not good for graphene or h-BN growth. We electrochemically polished the copper surfaces to form smooth substrates suitable for film growth. The copper foil was connected to the anode and placed in a solution (20 g potassium persulfate, 98%, and 500 mL DI water). A current of 1.0 A was applied over 5 min to remove the surface protective coating and to create a smooth copper foil surface. HF (20%) was then used to clean the copper surface and remove residual materials present after the previous polishing step. Finally, dry nitrogen gas was applied to dry the copper surface.

Synthesis process

Prior to BN/graphene monolayer/BN (BGB) film growth, the copper foil, prepared using the electrochemical polishing, was pre-annealed in the CVD chamber for 1 hour at 1050°C, under H_2 (70 sccm) and Ar (30 sccm) flows. The bottom h-BN film was grown by carrying the h-BN source (borazine) into the chamber in the N_2 carrier gas (0.5 sccm) under H_2 (5 sccm) and Ar (27 sccm) flows over 40 min. The graphene monolayer was subsequently grown directly on the h-BN/Cu substrate by introducing CH_4 (40 sccm), H_2 (40 sccm), and Ar (40 sccm) gases into the chamber for 40 min. Finally, the top BN layer was grown on the graphene monolayer/h-BN/Cu structure using the same growth parameters used to prepare the bottom h-BN, with different growth times of 20 min, 40 min, and 60 min.

Transfer process

A typical transfer method was used to transfer the h-BN, graphene monolayer/h-BN, or BGB films from the copper foil to other substrates, such as quartz, SiO_2/Si substrates, or Si_3N_4 TEM grids. First, PMMA (A6) was spin-coated onto the film surface to cover and protect the film during the transfer process. After coating, the sample was placed on a hot plate with a temperature of 90°C for 5 min to solidify the PMMA. Plasma etching was applied (O_2, 5 sccm) to clean the backside of the copper foil. The samples were then dumped into the copper etchant (iron (III) chloride solution (concentration of 0.1 g mL^{-1})) to etch away the copper over 12 hour, followed by rinsing twice with DI water. This film was then placed in HCl (10%) for 15 min to remove chemical residues, followed by rinsing with DI water to clean away the HCl. Finally, the film was ready for transfer onto the substrates. During film transfer onto the substrate, the film was placed on a hot plate with a temperature of 120°C for 5 min to re-solidify the PMMA. The film was then dumped into acetone at 50°C (heated by a hot plate) for 5 min to remove PMMA.

Results and discussion

The *in-situ* growth of BN layers on a graphene/h-BN/copper substrate was accomplished by sequentially growing large-area graphene/h-BN films on copper, as described previously.[9] A BN source (borazine) was then introduced into the growth

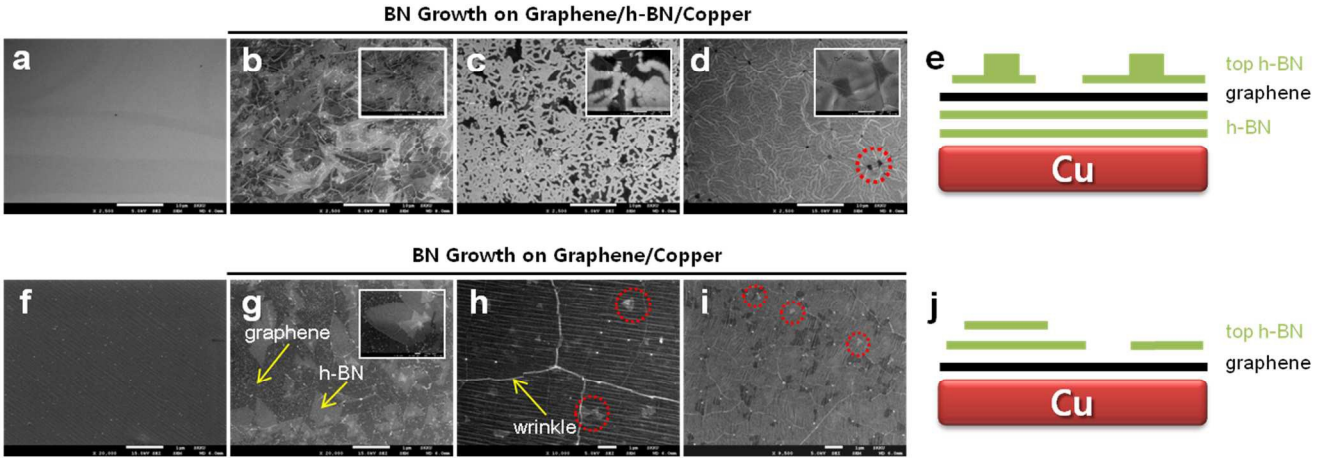

Fig 1. The difference of top BN growth on a graphene/h-BN/copper and a graphene/copper. (a) is the SEM image of graphene on copper, and (b)-(d) are the SEM images of 20, 40 and 60 minutes of top BN growth on a graphene/copper substrate of (a). (e) is a schematic for (c). (f) is the SEM image of graphene/h-BN/copper, and (g)-(i) are the SEM images of 20, 40 and 60 minutes of top BN growth on a graphene/h-BN/copper substrate of (f). (j) is a schematic for (h). All the insets are the magnified images of each corresponding image.

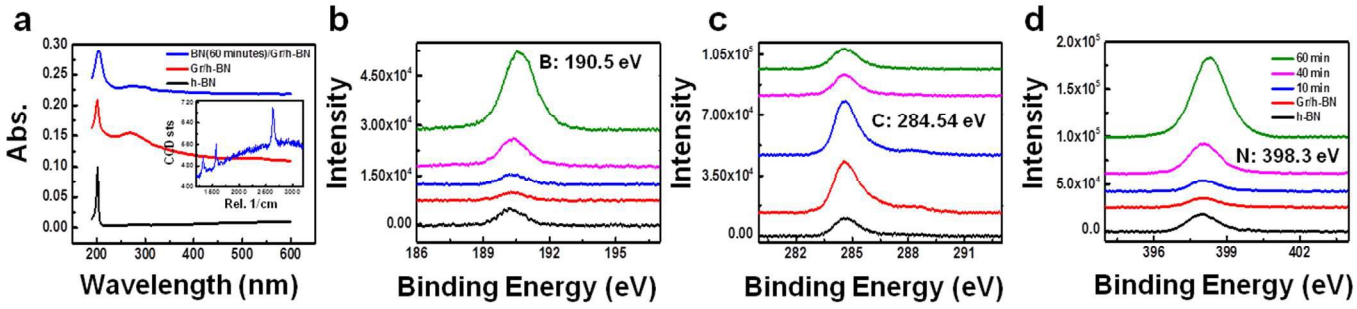

Fig. 2. The chemical analysis of an initial h-BN film, an intermediate graphene/h-BN film and a final BGB film. (a) is UV absorption spectra for three different samples of h-BN film (black), graphene/h-BN (red) and BN/graphene/h-BN (blue). And the inset image is the Raman spectra of BN/graphene/BN sample after transferring onto SiO_2 substrate; (b)-(d) are the XPS spectra for B, C and N of h-BN, graphene/h-BN, BN (20 min)/graphene/h-BN, BN (40 min)/graphene/h-BN and BN (60 min)/graphene/h-BN films.

chamber using N_2 as the carrier gas. The top BN growth process was monitored during the growth of the top BN layer over various growth times: 0 min, 10 min, 40 min, and 60 min, as shown in the SEM images of **Figures 1** a–d. Initially, the graphene/h-BN/copper sample presented a very smooth surface (Figure 1a). After 10 min of top BN layer growth, the surface morphology began to display additional layered structures featuring lines of dot structures (bright spots in Figure 1b) and small triangle-shaped BN islands. The 40 min growth time (Figure 1c) produced a variety of thick and mixed line structures with quite uniform height of ~10 nm (Figure S1a-b), which were grown by merging the dot structures. These thick and mixed line structures dominated and evenly covered most of the surface. Finally, the thick line structures covered the entire area evenly with still similar thickness of ~10 nm after 60 min growth (Figure 1d and Figures S1c-d). The overall thickness of BGB films, therefore, is uniform (~12.3 nm), where thickness of bottom BN is ~2 nm and that of top BN is ~10 nm each. Figure 1e shows a schematic diagram of the BGB sample structure.

The growth of the top BN layer on the graphene/h-BN/copper substrate was further explored by growing a BN layer under the same growth conditions (growth time and gas flow) on a graphene/copper substrate without applying an intermediate h-BN layer. Immediately after a full-coverage graphene film had been synthesized on the copper substrate, a top BN layer was grown over different growth times under the gas flow conditions used for BN layer growth in the graphene/h-BN/copper substrate structure, as shown in Figures 1f–1i. A top BN layer growth time of 10 min on the graphene/copper substrate (Figure 1g) clearly revealed the presence of additional multi-layer structures with clear and smooth edges but without the dot structures in a line. These features differed somewhat from those shown in Figure 1b. Even at further growth times up to 40 or 60 min (Figures 1h–1i), the sample surface remained smooth and was covered with triangular layers of top h-BN without forming a line of dot structures. The top h-BN growth was compared with growth on the graphene/h-BN/copper surface, suggesting that the layer-by-layer growth of the top h-BN layer on the graphene/copper surface was actively facilitated by the catalytic effects of the graphene/copper surface, and these effects were much less on the graphene/h-BN/copper surface. It was reported previously that, as the h-BN layer thickness on the copper increased, the catalytic effects of direct graphene growth decreased.[11] Figure 1j shows a schematic diagram of the h-BN growth on the graphene/copper substrate.

The crystallinity and quality of the graphene and h-BN layers were investigated during BGB growth by transferring the samples onto quartz substrates for *ex situ* UV-visible absorption measurements. Figure 2a reveals that the initial h-BN film (black) was high quality, as indicated by the sharp and high peak at 201 nm. The graphene grown directly on h-BN (red) displayed a weaker h-BN peak, with a graphene peak at 265 nm, as reported previously.[9] The *in situ*-grown BGB film (60 min growth of the top BN layer, blue) showed that the BN peak broadened as the graphene peak weakened. The broad and weak h-BN peaks were attributed to the complex thick line structures on the top BN film. The AFM results (see the Supporting Information) indicated that the line structures of the top BN were 10.3 nm high and 670 nm wide, respectively. The inset in Figure 2a is the Raman spectra measured on a BGB film (60 min growth of top BN) after transferred on to a SiO_2 substrate. This Raman data clearly shows the intensity ratio of $I_{2D}/I_G \approx 2$ with a broad background of BN layers, which indicates that a high quality graphene monolayer survived well in the BGB film even after the sequential CVD growth for the top BN layer. The XPS data collected from the B and N elements present in the three sample types (see the legend in Figure 2d) agreed well with the UV results, revealing that the concentration initially decreased (red) with increasing graphene coverage and subsequently increased (blue, pink, and green), depending on the top BN coverage. The concentration of C varied inversely with the concentrations of B and N, indicating that the BGB sample was *in situ* synthesized on copper sequentially in a layer-by-layer manner.

The BGB surface morphology and crystallinity were further investigated using HR-TEM and SAED methods. Figure 3a shows the HR-TEM results obtained from a graphene/h-BN sample transferred onto a Si_3N_4 grid. The surface was clearly atomically smooth and displayed a Moiré pattern. Figure 3b shows that the edge of the sample featured layers at the bent part of the film. These results clearly indicated that the graphene/h-BN film retained its layered structure, as reported previously.[9] Figure 3c shows the SAED image corresponding to the sample described in Figure 1a, collected from the graphene and h-BN layers. Figure 3d shows an HR-TEM image of a BN(40 min)/graphene/h-BN sample, in which the thick line structures of the top BN appeared darker. SAED images collected from the regions of the surface with or without the BN line structures are shown in Figures 3e and 3f, respectively. The SAED patterns obtained from the thick line structures of the top BN layer (blue) included additional rings with two sets of six-fold symmetric spots, indicating that the thick line structures of the top BN layer were poorly crystalline. The top

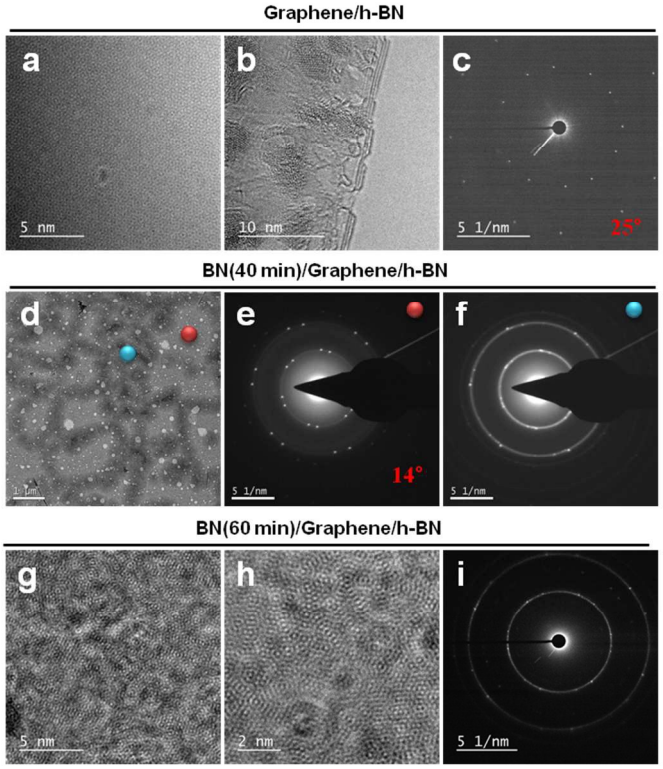

Fig. 3. TEM and SAED measurements to confirm the sample crystalline and surface morphology. (a) is the TEM image of a graphene/h-BN film after transferring onto a Si_3N_4 grid. (b) is the TEM image at the edge of the graphene/h-BN film, which clearly shows layered structures; (c) is the corresponding SAED data of (a), where the twisted angle between graphene and a h-BN film is 25°. (d) is the TEM image of a BN (40 min)/graphene/h-BN film. (e)-(f) are the corresponding SAED data at the red and blue dots in (d); (g)-(h) is the TEM image of a BN (60 min)/graphene/h-BN film. (i) is the corresponding SAED image of (h).

BN layer grown over 60 min revealed a top surface (Figures 3g–3h) that was smooth and fully covered with a thick BN layer, as shown in Figure 1d. Figure 3i shows the corresponding SAED image, which reveals clear dots patterns and a white ring corresponding to the thick line structure region shown in Figure 3f. Boron nitride can have different crystalline structures such as hexagonal BN (h-BN), cubic BN (c-BN, zinc blend structure), wurtzite BN (w-BN) and rhombohedral BN (r-BN). If the radius of the rings in SAED and the stability of BGB in air at room temperature, two similar structures of h-BN and r-BN are allowed with poor crystallinity of random orientations. The difference of those two crystalline structures is only stacking order. The morphology of the top BN is complicate even with quite uniform thickness. It is, therefore, hard to conclude the exact crystalline structure in this work.

Figures 4a and 4b show representative transfer characteristics collected from two distinct graphene field effect transistors (GFETs) over time. The characteristics presented in Figure 4a were obtained from a graphene monolayer protected by the top and bottom BN layers (BGB), and the characteristics presented in Figure 4b were obtained from a graphene monolayer without the top and bottom BN layers. The GFETs were fabricated using standard processes involving photolithography, electron-beam evaporation, and metal lift-off. Ti/Au (5/60 nm thick) source and drain electrodes were patterned on each film. The carrier transport characteristics were measured using a

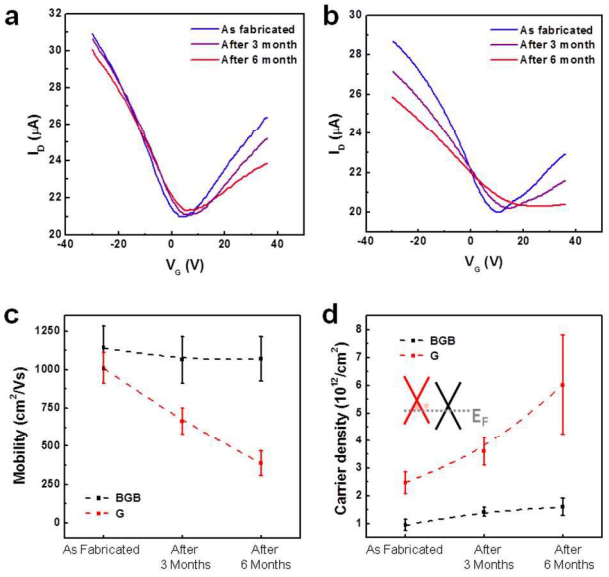

Fig. 4. Device experiments to confirm the robust quality of BN(60 min)/graphene/h-BN films in air. (a)-(b) are the IV curves of (a) graphene encapsulated with top and bottom h-BN films (BN/graphene/h-BN), and (b) graphene without a top protective film (graphene/h-BN). All the lines are color coded with the air exposure time; as fabricated (blue), after 3 month (purple), after 6 month (red). (c) is the field effect mobility, and (d) is the induced carrier concentration of GFETs as a function of air exposure time. Encapsulated graphene (black) clearly shows much more stable performance even after 6 months in ambient condition, while graphene without a top protective h-BN film does not.

semiconductor parameter analyzer (Keithley 4200-SCS). The protective effects of the top and bottom BN encapsulation layers on the graphene properties were investigated by measuring the characteristics immediately, 3 months, and 6 months after fabrication, with the aging conducted under ambient conditions. As the aging time increased, the characteristics of the encapsulated graphene did not degrade. Symmetric electron and hole transport, a constant I-V characteristic slope, and a constant Dirac point were observed. By contrast, the corresponding properties measured in graphene prepared without protective top BN layers were seriously degraded, and electron conduction could not be measured after 6 months.

The field effect mobilities, one of the most important parameters of those two types of GFETs, are shown in Figure 4c. The field effect mobility is given by the equation $\mu_{eff} = (L/W)\times(1/C_{ox}V_{ds})\times(\Delta I_{ds}/\Delta V_g)$, where L/W = 1 is the channel dimension, $C_{ox} = 1.2 \times 10^{-4}$ Fm^{-2} is the gate oxide capacitance per unit area ($C_{ox} = \varepsilon_0\varepsilon_r/d$; $\varepsilon_r = 3.9$; d = 285 nm), $V_{ds} = 0.1$ V is the drain–source voltage, and $\Delta I_{ds}/\Delta V_g$ is the current/voltage slope extracted from transfer characteristic. The mobility calculated from the BGB device decreased by 10% over the 6 months aging period under ambient conditions, whereas the mobility of graphene prepared without protective BN layers decreased by 70%. The doping effects due to aging were investigated by calculating the induced carrier concentration in each device, as shown in Figure 4d. The initially measured mobility in BGB devices is about ~1,200 cm^2/Vs typically. This limited value of graphene mobility is believed to come from the imperfect surface of the bottom BN layer with domain boundaries and possible vacancies. The induced carrier

concentration, n, was estimated from the Dirac point: $n = C_{ox}V_{Dirac}/e$, because the quantum capacitance of graphene was negligible on the 285 nm SiO_2. As protected from gas molecules (mainly H_2O and O_2) with top and bottom BN layers, graphene in BGB (black line in Figure 4d) did not display p-doping or degraded electrical properties over time, unlike graphene in a device prepared with graphene only (red line in Figure 4d).[12]

The h-BN layer is an ideal material for supporting or protecting graphene because it is atomically flat, provides a very small lattice mismatch, and is free from dangling bonds.[5] Graphene present in the sequentially synthesized BGB films, therefore, is mechanically robust, chemically inert, and devoid of impurities at the interface between the graphene and BN layers, even given the harsh transfer processes.[9] The dominant scattering sources in graphene typically correspond to charge impurities. The high κ measured from the h-BN (κ=6) layers, indicated that the carriers in graphene were not significantly affected by charge impurities in the bulk of the dielectric layer (h-BN), and the electrical performance of graphene encapsulated by BGB films may be improved by suppressing charge impurity scattering.[13,14]

Conclusions

In conclusion, we successfully synthesized a large-area graphene monolayer protected by in situ-grown top and bottom BN layers via low-pressure CVD. This approach eliminated the deleterious effects of mechanical transfer processes and the long exposure times in air. The crystallinity of each layer in the BGB sample was confirmed using HR-TEM and SAED measurements, which revealed that the top BN layer was amorphous. The SEM and HR-TEM surface morphology data indicated that the growth mechanism of the top BN layer corresponded to the Frank van der Merwe-like model: a layered structure grew initially, followed by island structure growth (in this case, indicated by the line structures). This type of BGB sample could be transferred onto a SiO2 substrate for device fabrication, and surprisingly, the electrical properties, Dirac point, and mobility did not change in air, even after a six-month aging process. The in situ-grown BN/graphene monolayer/h-BN films were mechanically robust, and the graphene layer in the heterostructure was chemically inert. The electrical performances, therefore, were extremely stable, suggesting that this approach may be useful for commercial applications involving graphene-based electronics.

Acknowledgements

This research was supported by the Institute for Basic Science (IBS) and Basic Science Research Program through the National Research Foundation of Korea (NRF) funded by the Korean government (MSIP) (Grant Numbers: IBS-R011-D1, 2011-0030046, 2012R1A1A1041416, NRF-2014M3C1A3001208, 2009-0083540 and 2013M3A6B1078873).

Notes and references

[1]SKKU Advanced Institute of Nanotechnology (SAINT), Sungkyunkwan University (SKKU), Suwon 440-746, Korea.

[2]Nano Electronics Lab., Samsung Advanced Institute of Technology, Suwon 443-803, Korea.

[3]Department of Chemistry, Sungkyunkwan University (SKKU), Suwon 440-746, Korea.

[4]Center for Integrated Nanostructure Physics, Institute for Basic Science (IBS), Sungkyunkwan University, Suwon 440-746. Korea.

[5]Center for Human Interface Nanotechnology (HINT), Sungkyunkwan University (SKKU), Suwon 440-746, Korea.

[6]College of Information and Communication, Sungkyunkwan University (SKKU), Suwon 440-746, Korea.

[7]Department of Physics, Sungkyunkwan University (SKKU), Suwon 440-746, Korea.

* Corresponding authors: yjsong@skku.edu (YJS); leesj@skku.edu (SL); leeyoung@skku.edu (YHL), Sungkyunkwan University (SKKU), Suwon 440-746, Korea.

Electronic Supplementary Information (ESI) available: [The thickness and width of BN lines in BN(40 min)/Graphene/BN sample and the thickness of the BN(60 min)/Graphene/BN sample, after transferring onto SiO_2 substrate, is discussed in detail].

1 A. K. Geim and I. V. Grigorieva, *Nature*, 2013, **499**, 419–425.
2 X. Hong, J. Kim, S.-F. Shi, Y. Zhang, C. Jin, Y. Sun, S. Tongay, J. Wu, Y. Zhang and F. Wang, *Nat. Nanotechnol.*, 2014, **9**, 682–686.
3 R. Quhe, J. Zheng, G. Luo, Q. Liu, R. Qin, J. Zhou, D. Yu, S. Nagase, W.-N. Mei, Z. Gao and J. Lu, *NPG Asia Mater.*, 2012, **4**, e6.
4 C.-H. Lee, G.-H. Lee, A. M. van der Zande, W. Chen, Y. Li, M. Han, X. Cui, G. Arefe, C. Nuckolls, T. F. Heinz, J. Guo, J. Hone and P. Kim, *Nat. Nanotechnol.*, 2014, **9**, 676–681.
5 C. R. Dean, A. F. Young, I. Meric, C. Lee, L. Wang, S. Sorgenfrei, K. Watanabe, T. Taniguchi, P. Kim, K. L. Shepard and J. Hone, *Nat. Nanotechnol.*, 2010, **5**, 722–726.
6 G.-H. Lee, Y.-J. Yu, X. Cui, N. Petrone, C.-H. Lee, M. S. Choi, D.-Y. Lee, C. Lee, W. J. Yoo, K. Watanabe, T. Taniguchi, C. Nuckolls, P. Kim and J. Hone, *ACS Nano*, 2013, **7**, 7931–7936.
7 J. Zhang, P. Chen, B. Yuan, W. Ji, Z. Cheng and X. Qiu, *Science*, 2013, **342**, 611–614.
8 Z. Liu, L. Song, S. Zhao, J. Huang, L. Ma, J. Zhang, J. Lou and P. M. Ajayan, *Nano Lett.*, 2011, **11**, 2032–2037.
9 M. Wang, S. K. Jang, W.-J. Jang, M. Kim, S.-Y. Park, S.-W. Kim, S.-J. Kahng, J.-Y. Choi, R. S. Ruoff, Y. J. Song and S. Lee, *Adv. Mater.*, 2013, **25**, 2746–2752.
10 H. H. Kim, Y. Chung, E. Lee, S. K. Lee and K. Cho, *Adv. Mater.*, 2014, **26**, 3213–3217.
11 M. Wang, M. Kim, D. Odkhuu, N. Park, J. Lee, W.-J. Jang, S.-J. Kahng, R. S. Ruoff, Y. J. Song and S. Lee, *ACS Nano*, 2014, **8**, 5478–5483.
12 Z. H. Ni, H. M. Wang, Z. Q. Luo, Y. Y. Wang, T. Yu, Y. H. Wu and Z. X. Shen, *J. Raman Spectrosc.*, 2009, **41**, 479–483.
13 F. Chen, J. Xia, D. K. Ferry and N. Tao, *Nano Lett.*, 2009, **9**, 2571–2574.
14 L. A. Ponomarenko, R. Yang, T. M. Mohiuddin, M. I. Katsnelson, K. S. Novoselov, S. V. Morozov, A. A. Zhukov, F. Schedin, E. W. Hill and A. K. Geim, *Phys. Rev. Lett.*, 2009, **102**.